

Denoising and Segmentation of 3D Brain Images

M. Vatsa¹, R. Singh¹, and A. Noore²

¹IIT Delhi, India, {mayank, rsingh}@iitd.ac.in

²West Virginia University, Morgantown, USA, afzel.noore@mail.wvu.edu

Abstract— *This paper presents an algorithm for medical 3D image denoising and segmentation using redundant discrete wavelet transform. First, we present a two stage denoising algorithm using the image fusion concept. The algorithm starts with globally denoising the brain images (3D volume) using Perona Malik’s algorithm and RDWT based algorithms followed by combining the outputs using entropy based fusion approach. Next, a region segmentation algorithm is proposed using texture information and k-means clustering. The proposed algorithms are evaluated using brain 3D image/volume data. The results suggest that the proposed algorithms provide improved performance compared to existing algorithms.*

Keywords: Medical Image Analysis, Denoising, Segmentation, Redundant Discrete Wavelet Transform

Typically, the field of medical image analysis involves: *post-acquisition* such as denoising and restoration, *segmentation* i.e. delineating features of interest, *registration*, i.e. align captured image with a model or previously captured image, *computation* i.e. physical quantity derivation, *visualization*, and *security*. Existing algorithms in medical image analysis, in general, use partial differential equations, curvature driven flows and different mathematical models. Wavelet based methods have also been proposed for medical image analysis. In 1991, Weaver et al. [1] first proposed the use of wavelet theory in medical imaging with the application to noise reduction in MRI images. Thereafter, several algorithms have been proposed for denoising, segmentation, reconstruction, functional MRI, registration, and feature extraction using continuous wavelet transform (CWT), discrete wavelet transform (DWT), and redundant DWT (RDWT). Detailed survey of wavelet based algorithms for medical imaging can be found in [2] [3], [4], and [5].

In this paper, we propose algorithms for brain image denoising and region based segmentation using RDWT for improved performance. RDWT [6], [7], also known as shift invariant wavelet transform, has proven its potential in different signal processing applications but it is not well researched in the field of medical image analysis. The proposed algorithms utilize properties of RDWT such as shift invariance and noise persubband relationship along with other techniques such as soft thresholding, clustering, and entropy for improved performance. Experimental results on the brain data show the usefulness of the proposed denoising and segmentation algorithms and clearly indicate

their potential in medical image analysis. Section 2 briefly explains the fundamentals of redundant discrete wavelet transform. Medical image denoising algorithm is explained in Section 3 and Section 4 describes the proposed image segmentation algorithm.

1. Shift Invariant Redundant Discrete Wavelet Transform

Generally, DWT [6], [8] is used in wavelet based medical image analysis as it preserves frequency information in stable form and allows good localization both in time and spatial frequency domain. However, one of the major drawbacks of DWT is that the transformation does not provide shift invariance. This causes a major change in the wavelet coefficients of the image even for minor shifts in the input image. In medical imaging, we need to know and preserve exact location of different information; but shift variance may lead to inaccuracies. For example, in medical image denoising it is important to preserve edge information and remove noise, but DWT based denoising may produce specularities along the edges. Several techniques have been proposed to address shift variance in denoising and segmentation [9].

In this paper, we use RDWT [6], [7], [10] to overcome the shift variance problem of DWT. RDWT can be considered as an approximation to discrete wavelet transform that removes the down-sampling operation from traditional critically sampled DWT, produces an overcomplete representation, and provide noise persubband relationship [7]. The shift variance of DWT arises from the use of down-sampling whereas RDWT is shift invariant because the spatial sampling rate is fixed across scale. Similar to DWT, RDWT and Inverse RDWT (IRDWT) of a two dimensional image or three dimensional volume data is obtained by computing each dimension separately where detailed and approximation bands are of the same size as the input image/data ¹.

2. Fusion based Two Stage Approach to Medical Image Denoising

This section presents a fusion based denoising algorithm that utilizes the concept of image fusion. In this two stage approach, we first concurrently apply two denoising algorithms

¹Mathematical details of RDWT can be obtained from [6] and [7]. For the proposed algorithms, we use Db9/7 mother wavelet.

globally and then, in the second stage, generate the quality enhanced image by locally combining the good quality regions from the two denoised images. In this research, we use Perona Malik's algorithm [11] and RDWT based denoising algorithm as the two ingredient algorithms and the outputs of these two algorithms are combined using the proposed fusion technique. This section first describes the RDWT based denoising algorithm followed by the fusion approach.

2.1 RDWT base Image Denoising

Let I_T be the true image and N be the noise component. As described by Jin et al. [2], the relationship of noisy image I_N corresponding to I_T and N can be written as

$$I_N = I_T + N \quad (1)$$

Denoising I_N using wavelet transform to recover the true signal I_T can be represented as,

$$I_R = \sum_i W(I_N, l, t) \quad (2)$$

where I_R represents the reconstructed signal, W represents the wavelet based denoising, l represents the level of decomposition, and t is the function that aims at eliminating noise components in the transform domain while preserving the true signal coefficients. In ideal conditions, $I_R = I_T$. DWT based denoising algorithms have been proposed in [12]-[13] using different wavelet basis and thresholding schemes. All these algorithms use some technique to handle shift variance but suffer due to presence of visual artifacts and Gibbs phenomenon. Here, we use RDWT in the proposed denoising algorithm to address shift invariance and challenges due to artifacts.

I_N is decomposed at l levels using 3D/2D RDWT. Soft thresholding technique [14] is applied on the RDWT coefficients of subband C_i ($i = 1, 2, \dots, l$) with threshold t_i to obtain the denoised subband C'_i .

$$C'_i(x) = \begin{cases} x - t_i, & \text{if } x \geq t_i \\ x + t_i, & \text{if } x \leq -t_i \\ 0, & \text{if } |x| < t_i \end{cases} \quad (3)$$

where the threshold for each subband t_i is computed using Equation 4.

$$t_i = \frac{S\alpha_i^2}{\sigma_i} \quad (4)$$

Here, σ_i is the standard derivation for the i^{th} subband and the noise variance for each subband, α_i^2 , is computed using Equation 5,

$$\alpha_i^2 = \left[\frac{\text{median}(C_i)}{0.6745} \right]^2 \quad (5)$$

The scale parameter S is computed using L_m , i.e length of subband at m^{th} scale,

$$S = \sqrt{\log\left(\frac{L_m}{l}\right)} \quad (6)$$

Finally, the medical volume/image is reconstructed by applying 3D/2D IRDWT on C'_i to get the denoised medical data.

2.2 Combining the Output of Perona Malik and RDWT Algorithms

As mentioned previously, in the proposed fusion based algorithm, the noisy image I_N is first denoised using Perona Malik's and RDWT based algorithms to obtain I_P and I_R respectively. Next, image fusion is performed to combine I_P and I_R to further enhance the image which provides I_F .

Three level of RDWT decomposition is applied on I_P and I_R to obtain the detail and approximation RDWT subbands. Let I_P^a, I_P^v, I_P^d , and I_P^h be the RDWT subbands from I_P and I_R^a, I_R^v, I_R^d , and I_R^h be the corresponding RDWT subbands from the I_R image. To preserve the features from both the images, coefficients from the approximation band of I_1 and I_2 are averaged,

$$I_F^a = \text{mean}(I_P^a, I_R^a) \quad (7)$$

where I_F^a is the approximation band of the fused image. For the three detailed subbands, each band is divided into blocks of size 3×3 and the entropy of each block is calculated using Equation 8.

$$e_i^{jk} = \ln \sqrt{\left(\frac{\mu_i^{jk} - \sum_{x,y=1}^{3,3} I_i^{jk}(x,y)}{\sigma_i^{jk}} \right)^2} / m \quad (8)$$

where j ($= v, d, h$) denotes the subbands, $m = 3$ (size of each block), k represents the block number, and i ($= P, R$) is used to differentiate between two globally denoised images I_P and I_R . μ_i^{jk} and σ_i^{jk} are the mean and standard deviation of the RDWT coefficients where k represents the block, j represents the subband and i is the image. The detail subbands for the fused image I_F^v, I_F^d , and I_F^h , are generated using the entropy values as shown in Equation 9. For fused image block I_F^{jk} , RDWT coefficients from I_P is selected if the entropy of block from image I_P is greater than the entropy of corresponding block from image I_R , otherwise I_R^{jk} is selected.

$$I_F^{jk} = \begin{cases} I_P^{jk}, & \text{if } (e_P^{jk}) > (e_R^{jk}) \\ I_R^{jk}, & \text{otherwise} \end{cases} \quad (9)$$

Finally, IRDWT is applied on the four fused subbands to generate the final enhanced image I_F .

$$I_F = \text{IRDWT}(I_F^a, I_F^v, I_F^d, I_F^h) \quad (10)$$

Figure 1 shows the 90th slice of the denoised 3D brain volume [15] and Figure 2 shows a comparative illustration of the denoising algorithms.

3. Medical Image Segmentation using RDWT Entropy Features

Segmentation of biomedical images is the basis for 3D visualization and operation simulation. Precision in segmentation is critical to diagnosis and treatment. Conventionally, segmentation methods are divided into region based segmentation and edge or gradient based segmentation. Region based segmentation [16], [17] is usually based on the concept of finding similar features such as brightness and texture patterns. Edge based segmentation methods [18] are based on finding the high gradient value in the image and then connect them to form a curve representing a boundary of the object.

In this section, we propose RDWT based medical image segmentation algorithm which is a region-based method but inherently provides the features of edge-based segmentation method too. Since the detail bands of RDWT decomposed image provide gradient information, we can use these information for region segmentation. The proposed region based segmentation algorithm is described as follows:

Let I be the medical image/volume data to be segmented. This image is decomposed into n levels using RDWT. The proposed approach uses the wavelet energy features computed from the approximation band and all the detailed bands using block size of $x \times x$, where $x \leq 3$ (In our experiments, we chose the block size as 3×3). f_i , the energy features for RDWT subbands (where $i = \{a, h, v, d\}$ and a - approximation, v - vertical, d - diagonal, h - horizontal), are computed using Equations 11.

$$f_i = \left(\frac{1}{x} \sum_j \sum_k C_{ijk}^2 \right)^2 + \frac{1}{x} \sqrt{\frac{\mu_i^{jk}}{\sigma_i^{jk}}} \quad (11)$$

These energy features, f_a, f_v, f_d , and f_h , reflect the texture property of an image, and the wavelet energy features computed from detailed subbands provide the gradient information which facilitates the robust segmentation. Further, we use k -means clustering based learning algorithm which first learns from the training data and then identifies different feature regions at the testing time. Training data is used to train the k -means clustering algorithm [19] and form different clusters or groups of brain regions such as background, skull, and fat. As shown in Figure 3, we consider six regions present in the brain image namely, background, CSF, grey matter, white matter, skull, and fat. k -means clustering algorithm is trained using the simulated brain data as training data and different colors are assigned to the clusters. For segmentation, the test image is first decomposed into $n = 3$ levels and wavelet energy features are computed

for every level. For the n^{th} level, trained k -means algorithm classifies every feature and assigns a color to each feature. The segmented subbands are reconstructed to get the $n - 1$ level of segmented decomposition. At this point of time, approximation band is the segmented image obtained from previous step and detailed subbands are non-segmented. The same procedure is applied till the reconstruction reaches to 0th level which gives the final segmented image. This algorithm uses the concept of multi-resolution analysis since the results of n^{th} level are used to compute the results of $(n - 1)^{\text{th}}$ level. Figure 4 shows the segmentation results on the brainweb database.

4. Experimental Evaluation

To evaluate the performance of the proposed denoising and segmentation algorithms, we use the 3D Brainweb database [15]. This database contains images with different noise factors along with the ground truths. To quantitatively evaluate the denoising algorithm, Mean Square Error (MSE) and Structural Similarity Metrics (SSIM) [20] are used. Table 1 delineates the experimental results for the proposed denoising algorithm. Using the ground truth and noisy images with 7% noise, MSE is 121.4500 and SSIM is 0.5613 whereas with 9% noise, MSE is 189.6959 and SSIM is 0.5040. Denoising algorithm should decrease the MSE and increase the SSIM values. On applying Perona Malik's denoising algorithm [11] to the 7% noisy brain volume, MSE is reduced to 93.9106 and SSIM is increased to 0.6449 whereas with the RDWT based denoising algorithm, MSE is 88.3808 and SSIM is 0.6494. Compared to existing algorithms, the proposed fusion based algorithm significantly improves the visual quality of the brain image. This observation also holds with the 9% noisy brain data (Table 1). These results also suggest that the Perona Malik's denoising algorithm and RDWT based denoising algorithm provide complementary information and the fusion approach combines the globally denoised images such that the fused information provide better quality image. An interesting observation is related to the time taken to denoise the image. With Perona Malik's algorithm, time to denoise the image is very much dependent on the amount of noise present in the image. With RDWT based denoising algorithm, computational requirement is reduced because of inherent advantages of shift invariance and able to tolerate noise. For fusion based approach, the computational time includes time to globally denoise the brain image and to fuse the denoised images. Although the computational time for fusion approach is higher than constituent algorithms but the visual quality is significantly increased, thereby making it applicable to medical applications.

Next, correct classification accuracy is used to evaluate the segmentation algorithm. Figure 5 shows a close view of the segmentation result. Visually, the results are encouraging and preserve both the region and edge information. Since the

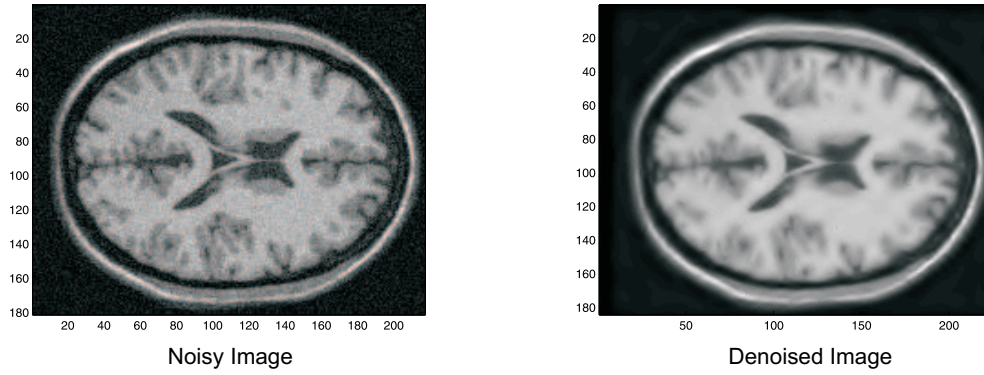


Fig. 1: Denoising medical data using RDWT based algorithm.

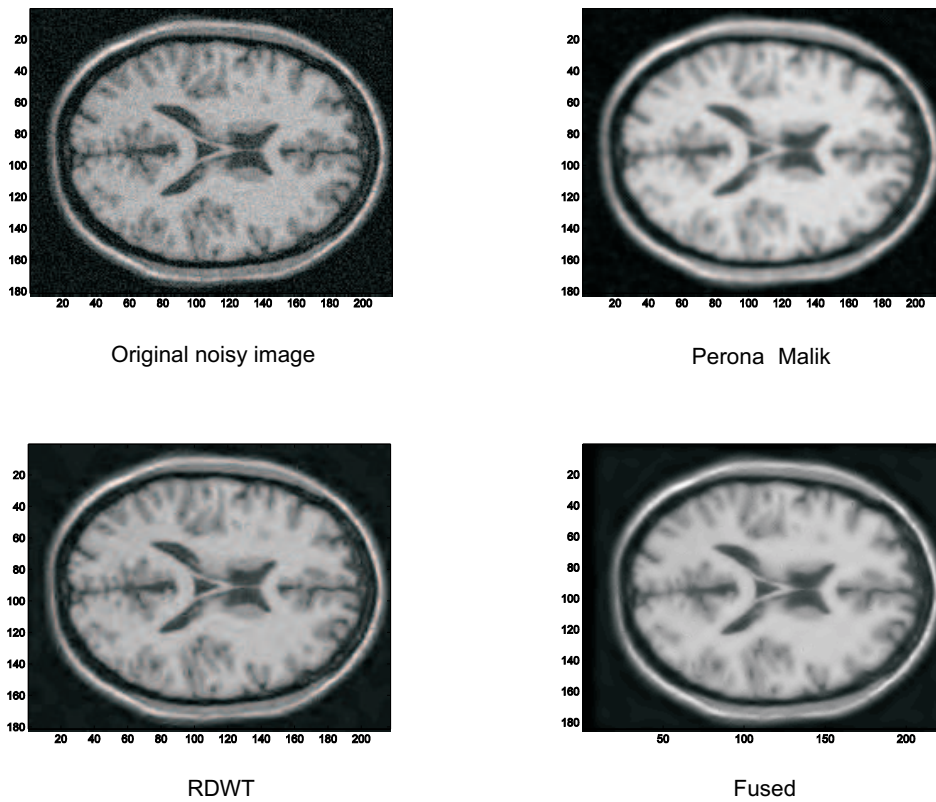


Fig. 2: Comparison of Denoising algorithms.

Table 1: Comparing the performance of denoising algorithms on the 3D brainweb database

Algorithm	Noise Factor (%)	MSE	SSIM	Time (Sec.)
Noisy Image	7	121.4500	0.5613	—
	9	189.6959	0.5040	—
Perona Malik	7	93.9106	0.6449	36.29
	9	143.2438	0.6084	75.54
RDWT	7	88.3808	0.6494	28.02
	9	134.1269	0.6188	52.14
Fusion	7	70.5161	0.7157	71.34
	9	119.2349	0.6525	138.35

Brainweb database provides the ground truth, correct classification accuracy quantitatively represents the performance of the segmentation algorithm. For the six categories or regions, Table 4 shows that the proposed algorithm provides the accuracy in the range of 91.9-94.8%. In comparison with the existing SVM based segmentation algorithm [21], the proposed algorithm yields similar results. However, the main advantage is with computational time. With the proposed algorithm, the time taken to segment the regions of 3D brain volume is 5.37 seconds (at an average) whereas with the

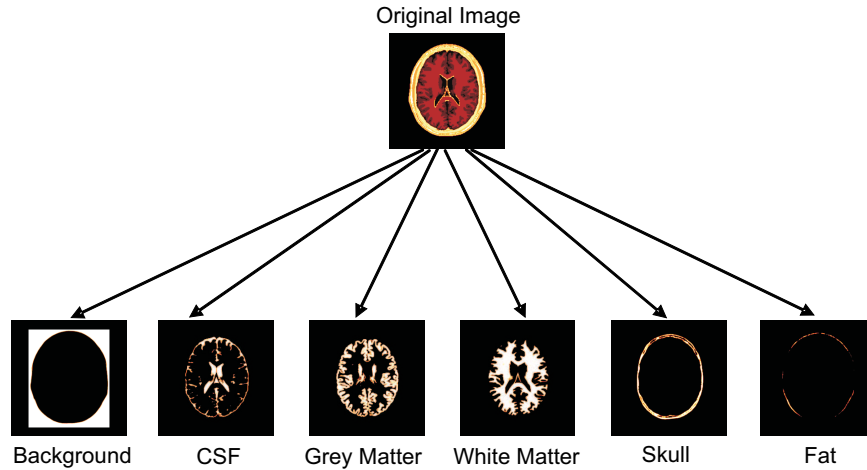


Fig. 3: Training data used for training the clustering algorithm.

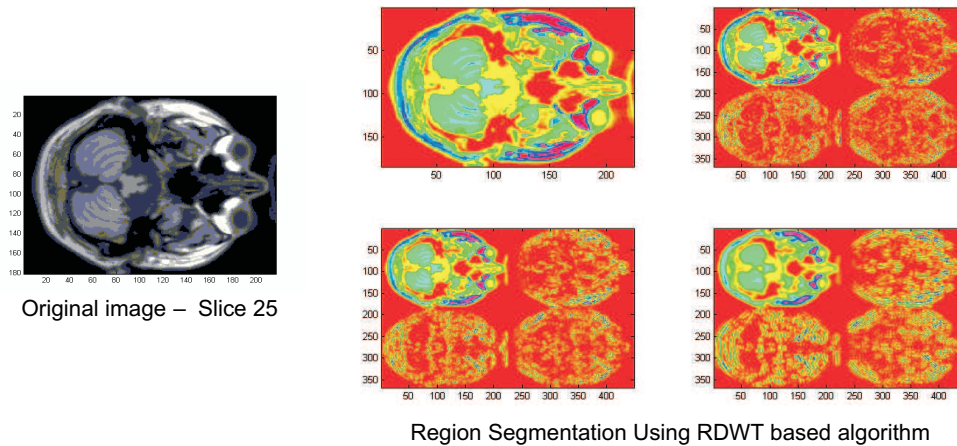


Fig. 4: Segmentation using RDWT based algorithm.

SVM based algorithm, it is 37.22 seconds.

Further, in another experiment, we segment the noisy brain data (Figure 6). It is clear from this result that the segmentation of noisy images yield erroneous results. However, when the brain image is first denoised and then segmented, the results show clear and correct segmentation. Furthermore, visual results were shown to eminent medical professionals and they asserted that the proposed denoising and segmentation algorithms provide better information compared to existing algorithms.

5. Conclusion

Computer assisted diagnosis and therapy, in general, require image processing operations such as denoising and segmentation. Sophisticated imaging techniques such as MRI and CAT scanning provide abundant information but require preprocessing techniques so that 3D image/volume can be optimally used for diagnosis. This paper presents fusion

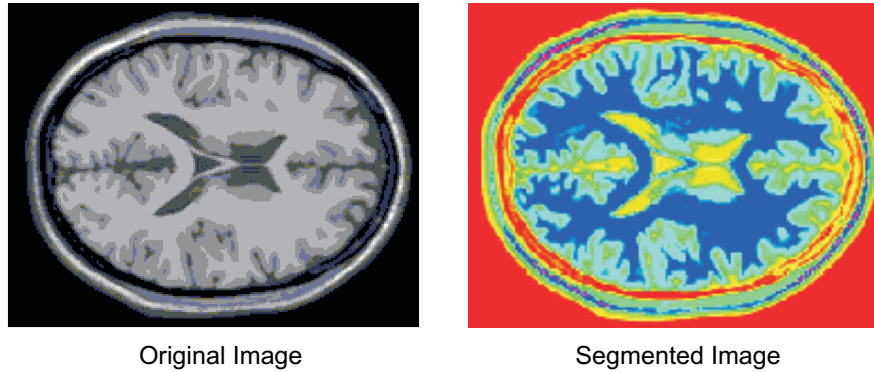
based denoising algorithm and RDWT entropy based region segmentation algorithm. Using the 3D Brainweb database, the proposed algorithms show significant improvement over existing algorithms. In future, fusion based denoising algorithm and segmentation will be extended with the non-linear learning approach for further reducing the errors.

6. Acknowledgment

The authors would like to thank McConnell Brain Imaging center, Montréal Neurological Institute, McGill University for providing Brainweb database. The authors also acknowledge medical professionals for providing insightful comments and suggestions.

References

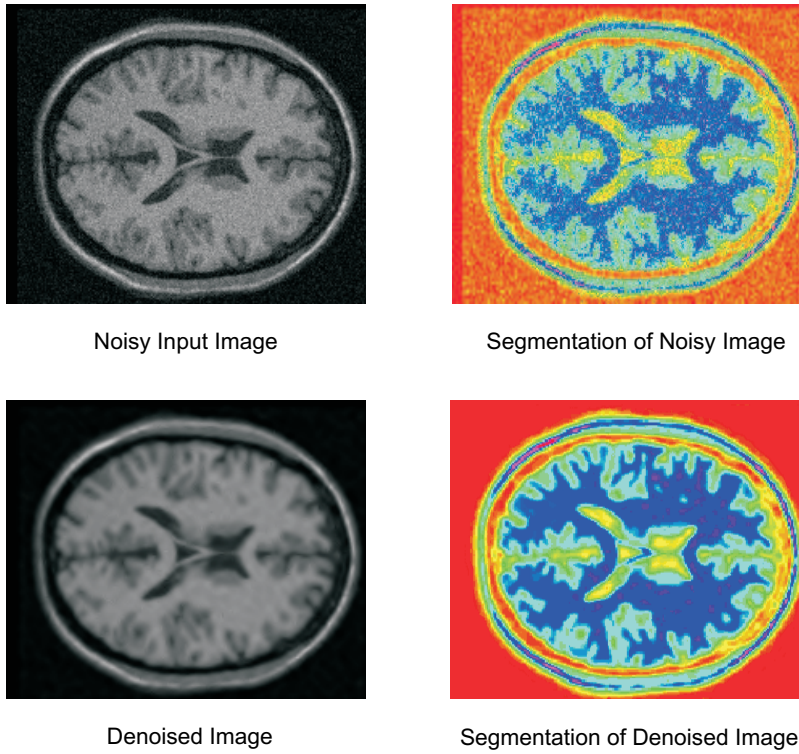
- [1] J. B. Weaver, X. Yansun, D. Healy, and L. D. Cromwell, "Filtering noise from images with wavelet transforms," *Magnetic Resonance in Medicine*, vol. 21, no. 2, pp. 288–295, 1991.



Original Image

Segmented Image

Fig. 5: A closer view of RDWT segmented brain image.



Noisy Input Image

Segmentation of Noisy Image

Denoised Image

Segmentation of Denoised Image

Fig. 6: Segmentation of noisy and denoised brain image.

Table 2: Correct classification accuracy of the segmentation algorithm.

Method	Background	CSF	Grey Matter	White Matter	Skull	Fat
SVM Segmentation [21]	94.1%	92.6%	93.2%	93.7%	91.5%	92.4%
Proposed	94.8%	92.6%	93.5%	93.6%	91.9%	92.4%

- [2] Y. Jin, E. Angelini, and A. Laine, "Wavelets in medical image processing: denoising, segmentation, and registration," *Handbook of Biomedical Image Analysis*, pp. 305–258, 2006.
- [3] A. Laine, "Wavelets in spatial processing of biomedical images," *Annual Review of Biomedical Engineering*, vol. 2, pp. 511–550, 2000.
- [4] M. Unser and A. Aldroubi, "A review of wavelets in biomedical applications," *Proceedings of the IEEE*, vol. 84, no. 4, pp. 626–638, 1996.
- [5] M. Unser, A. Aldroubi, and A. Laine, *IEEE Transactions on Medical Imaging: Special Issue on Wavelet's in Medical Imaging*, 2003.
- [6] I. Daubechies, *Ten lectures on wavelets*. Society for Industrial and Applied Mathematics, 1992.
- [7] J. Fowler, "The redundant discrete wavelet transform and additive noise," *IEEE Signal Processing Letters*, vol. 12, no. 9, pp. 629–632, 2005.
- [8] O. Rioul and M. Vetterli, "Wavelets and signal processing," *IEEE Signal Processing Magazine*, vol. 8, no. 4, pp. 14–38, 1991.
- [9] G. Beylkin, "On the representation of operators in bases of compactly supported wavelets," *SIAM Journal of Numerical Analysis*, vol. 29, pp. 1716–1740, 1992.
- [10] G. Strang and T. Nguyen, *Wavelet and filter banks*. Wellesly-Cambridge Press, 1996.
- [11] P. Perona and J. Malik, "Scale-space and edge detection using anisotropic diffusion," *IEEE Transaction on Pattern Analysis and Machine Intelligence*, vol. 12, no. 7, pp. 629–639, 1990.
- [12] E. Angelini, A. Laine, S. Takuma, J. Holmes, and S. Homma, "LV volume quantification via spatio-temporal analysis of real-time 3D echocardiography," *IEEE Transactions on Medical Imaging*, vol. 20, pp. 457–469, 2001.
- [13] Y. Jin, E. Angelini, P. Esser, and A. Laine, "De-noising SPECT/PET images using cross-scale regularization," *Proceedings of the Sixth International Conference on Medical Image Computing and Computer Assisted Interventions*, vol. 2879, no. 2, pp. 32–40, 2003.
- [14] D. Donoho, "De-noising by Soft-thresholding," *IEEE Transaction on Information Theory*, vol. 41, no. 3, pp. 613–627, 1995.
- [15] [Http://www.bic.mni.mcgill.ca/brainweb/](http://www.bic.mni.mcgill.ca/brainweb/).
- [16] D. H. Ballard and C. Brown, *Computer vision*. Prentice Hall, 1982.
- [17] A. Laine and J. Fan, "Frame representation for texture segmentation," *IEEE Transaction on Image Processing*, vol. 5, no. 5, pp. 771–780, 1996.
- [18] M.Kass, A.Witkin, and D.Terzopoulus, "Snakes: Active contour models," *International Journal of Computer Vision*, vol. 1, no. 4, pp. 321–331, 1988.
- [19] R. O. Duda, P. E. Hart, and D. G. Stork, *Pattern classification*. Willey, 2000.
- [20] Z. Wang, A. C. Bovik, B. R. Sheikh, and E. P. Simoncelli, "Image quality assessment: From error visibility to structural similarity," *IEEE Transaction on Image Processing*, vol. 13, pp. 500–512, 2004.
- [21] L. Guo, X. Liu, Y. Wu, W. Yan, and X. Shen, "Research on the segmentation of MRI image based on multi classification support vector machine," *Proceedings of the 29th Annual International Conference of the IEEE Engineering in Medicine and Biology Society*, pp. 6019–6022, 2007.